Investigation of the aerodynamic phenomena associated with a long lorry platoon running through a tunnel

Zhang, Xiaotian; Robertson, Francis; Soper, David; Hemida, Hassan; Huang, Shi-Di

DOI:
10.1016/j.jweia.2020.104514

Document Version
Peer reviewed version

Citation for published version (Harvard):
Zhang, X, Robertson, F, Soper, D, Hemida, H & Huang, S-D 2021, 'Investigation of the aerodynamic phenomena associated with a long lorry platoon running through a tunnel', *Journal of Wind Engineering and Industrial Aerodynamics*, vol. 210, 104514. https://doi.org/10.1016/j.jweia.2020.104514

Investigation of the aerodynamic phenomena associated with a long lorry platoon running through a tunnel

Xiao-Tian Zhang[a,b,c], Francis H. Robertson[a], David Soper[a], Hassan Hemida[a,*], Shi-Di Huang[b,c,*]

[a]*School of Engineering, University of Birmingham, Birmingham, B15 2TT, Edgbaston, UK*
[b]*Center for Complex Flows and Soft Matter Research and Department of Mechanics and Aerospace Engineering, Southern University of Science and Technology, Shenzhen, 518055, Guangdong, China*
[c]*Guangdong Provincial Key Laboratory of Turbulence Research and Applications, Southern University of Science and Technology, Shenzhen, 518055, Guangdong, China*

Abstract

In recent years, the concept of vehicle platooning has gained widespread attention for its highly efficient road usage and lower fuel consumption. However, the aerodynamics of vehicle platoons travelling in a tunnel are not well understood, even though more and more road tunnels have been built to alleviate the traffic congestion problem. This paper presents a detailed study of the aerodynamic flow created by a long lorry platoon running through a tunnel, conducted via a combination of model-scale experiments and Improved Delayed Detached Eddy Simulations (IDDES). The slipstream velocity and pressure, the lorry surface pressure, as well as the drag coefficient, were investigated systematically and compared with the results obtained in the open air. The results show greater pressure variations when the platoon is running through the tunnel. The piston effect in the tunnel leads to a lower approaching velocity and a weaker flow separation compared to the case in the open air. All vehicles, in both the tunnel and the open air, experience a drag reduction due to platooning. Interestingly, the drag reduction in the tunnel is 20% greater than that in the open air, implying a greater potential in fuel saving.

Keywords: Vehicle aerodynamics, Lorry platoon, Road tunnel, Model-scale experiment, IDDES, Drag reduction

1. Introduction

Road traffic has been continuously increasing over the years. For example,

* Corresponding authors

Email addresses: h.hemida@bham.ac.uk (Hassan Hemida), huangsd@sustech.edu.cn (Shi-Di Huang)

passenger transport in Europe increased by 8% from 2005 to 2015. To deal with the growing traffic demand and the consequent environmental problem due to increasing pollutant emissions, the concept of platooning has long been proposed as a potential solution (Shladover et al., 1991). Platooning, or vehicle convoys, refers to the case where several vehicles form a road-train, with relatively small gaps between vehicles that are maintained autonomously. Thanks to the recent fast development of autonomous road vehicles, the platooning strategy has once again become an important topic in both academic and industrial fields.

To date, most studies of the aerodynamics of vehicle platoons were conducted in the environment of open air (Alam et al., 2010; Armagan et al., 2015; Bonnet and Fritz, 2000; Browand et al., 2004; Davila et al., 2013; Humphreys and Bevly, 2016; Lammert et al., 2014; Le Good et al., 2018; Liang et al., 2016; McAuliffe and Ahmadi-Baloutaki, 2018; Pagliarella, 2009; Robertson et al., 2021, 2019; Schito and Braghin, 2012; Tsuei and Savaş, 2001; Watkins and Vino, 2008; Zabat et al., 1995). Based on these studies, it is now generally accepted that platooning can not only increase the efficiency of road utilisation but also bring other benefits, such as decreasing the drag coefficient and thus reducing the fuel consumption. For example, considerable drag reduction was identified by (McAuliffe and Ahmadi-Baloutaki, 2018) in their wind tunnel experiments of a two-truck platoon with various inter-vehicle separation distances. They also investigated the effect of crosswinds, vehicle configuration and vehicle stagger on the truck platoon. However, very few studies have focused on platoons with more than four vehicles, mainly due to the length limitation of wind tunnels and the high requirement of computational resources. It is not known *a priori* whether long platoons would behave similarly as the short ones. (Davila et al., 2013) conducted numerical simulations for a five-vehicle platoon with mixed vehicle shapes and confirmed that the aerodynamic drag coefficient is reduced for all the vehicles in that platoon configuration. (Le Good et al., 2018) investigated platoons of up to 5 cars and found an increase in drag under certain conditions, suggesting that the optimisation techniques for low-drag styles of vehicles depend on the platoon formation. Nevertheless, studies on platoons of bluff vehicles with square backs, such as lorries (albeit often conducted with fewer vehicles), seem to consistently show a reduction in drag due to platooning. More recently, (Robertson et al., 2019) carried out model-scale experiments to investigate the aerodynamics of a long platoon with eight lorries. It was found that the downwind lorries were shielded effectively, and they all experienced significant drag reductions. Their experimental work was also complemented with numerical simulations, which showed excellent agreement regarding the drag coefficients (He et al., 2019).

On the other hand, increasing numbers of road tunnels have been built in recent years to alleviate the urban traffic congestion problem (Chung and Chung, 2007). When vehicles are travelling in a tunnel, the presence of tunnel walls restricts the

airflow motions and additional aerodynamic forces act on the vehicles, which are likely to influence the drag coefficient and even the stability of the vehicles. Therefore, studying the aerodynamic phenomena associated with vehicles moving in a tunnel is crucial in the design and operation of road tunnels. Early studies of this issue mainly came from field measurements (Jang and Chen, 2002, 2000) and model-scale experiments (Chen et al., 1998; Sambolek, 2004). Due to the cost and limitations of experimental techniques, these studies generally focused on how time-averaged flow quantities, such as the mean drag coefficient, vary with the size, speed and number of the vehicles. The complete picture of the velocity and pressure fields, especially the transient aerodynamics when vehicles entering and leaving the tunnel, has largely been overlooked.

With the rapidly growing ability of computational methods to reliably and affordably simulate complex flows, Computational Fluid Dynamics (CFD) has become a powerful tool to reveal detailed flow dynamics around moving vehicles. Of the many different simulation approaches available, the Reynolds Averaged Naiver Stokes (RANS) equations with the $k-\varepsilon$ model is the most widely used in the academic literature, largely due to its comparatively low cost. (Li et al., 2009) used dynamic mesh techniques to numerically simulate the aerodynamics of one van running into a tunnel. They found that the drag coefficient increased sharply near the tunnel entrance, about 13% more than that in the open air. They later adopted the renormalisation group method (Yakhot and Orszag, 1986) to study the process of two vans running in a tunnel (Li et al., 2010). It was found that the aerodynamic characteristics around the first van were similar to that of a single van, and the aerodynamic forces on the truck behind did not have an obvious change. By performing a numerical study combining a one-dimensional mathematical model and a RANS simulation, (Wang et al., 2014) obtained similar results for the case of a two-vehicle platoon moving in a curved tunnel. They further found that the effective drag coefficient increased with increasing the inter-vehicle spacing but decreased with an increase in the vehicle speed, which was attributed to the influence of vehicle wake on the airflow. (Song and Zhao, 2019) also conducted RANS simulations to investigate the flow patterns induced by a fleet of vehicles inside a road tunnel. Their results showed that the drag coefficient fluctuated dramatically during the vehicle passing period, which could be attributed to the unstable traffic wind during the transient movement process.

However, many authors reported that while the predicted drag coefficients in vehicle aerodynamics are acceptable, the pressure distributions are often inaccurate. For example, (Humphreys and Bevly, 2016) pointed out that RANS modelling was only valid in predicting drag reduction for short platoons (with less than four vehicles), and its description of the flow field was far from satisfactory and sometimes non-physical. In addition, the one-dimensional model could result in either underestimating or overestimating the drag forces, depending on the traffic

conditions, e.g., the speed and number of the vehicles (Eftekharian et al., 2015). In this context, Detached Eddy Simulation (DES) is a more suitable numerical approach (Spalart et al., 1997). Indeed, some researchers have used DES to study platoon aerodynamics and obtained good agreement with experiments at a low computational cost compared to Large Eddy Simulation (LES) (He et al., 2019; Humphreys and Bevly, 2016). Nevertheless, previous simulation works pertaining to the phenomena of vehicle platoons in a tunnel have mostly been based on RANS in the academic literature, despite its deficiencies. Furthermore, as is the case in the open air, these studies were limited to relatively short platoons. Moreover, the traffic wind induced by vehicle platoons running in the tunnel ~~have~~ has been rarely studied. These limitations of the previous research form the motivation of the present study.

This paper aims to improve our understanding of the aerodynamic phenomena associated with a long vehicle platoon running through a tunnel. To achieve this goal, both model-scale experiments and numerical simulations were conducted, and the results are compared to a similar study conducted in the open air. The model-scale experiments were performed with novel moving models at the University of Birmingham Transient Aerodynamic Investigation (TRAIN) rig facility (Robertson et al., 2019). The slipstream properties and vehicle surface pressure were measured to provide a benchmark for validating the CFD results. For the numerical simulations, a sophisticated DES method (Gritskevich et al., 2012) was utilised ~~here~~ to obtain high-quality information of the unsteady flow. These results enable us for the first time to have a full understanding of the aerodynamic behaviour of a long platoon travelling through a tunnel. The rest of the paper is organised as follows. The TRAIN rig facility and the moving vehicle models are described in section 2.1, followed by the data analysis methodology in section 2.2. The numerical methods are specified in section 3. Section 4 presents a detailed analysis of the velocity and pressure fields, the vehicle surface pressure, and the drag coefficient. A comprehensive comparison between the behaviours of a vehicle platoon in the tunnel and in the open air will also be made in this section. Finally, the conclusions are presented in section 5.

2. Experiment methodology

2.1. Experimental set-up

A series of novel moving model-scale experiments were performed at the University of Birmingham TRAIN rig facility. The TRAIN rig facility is a purpose-built facility to examine transient aerodynamics of vehicles (Baker et al., 2001). The reduced-scale vehicle models can be propelled along a series of 150 m long tracks at speeds up to 75 m/s. They are fired by pre-tensioned elastic bungee ropes

without additional propulsion and then run at a relatively constant specified speed before decelerating by a friction device. More detail about the rig facility can be found in (Soper, 2016). In this work, eight lorry models in a platoon formation were supported by a long spine type system. Therefore, they can run as a single unit at the same speed and at a fixed inter-lorry spacing (Robertson et al., 2019). The ground plane was composed of two suspended plane halves with a minimised gap of 10 mm in width. The scaled tunnel with a rectangular cross–section in shape was built on the plane, with the length, width and height being 10 m, 0.26 m and 0.215 m, respectively. Figure 1 shows the photographs of the platform and the lorry platoon on the rig. Note that in Figure 1(b), the roof of the tunnel was temporally removed to show the lorries and cobra probes inside. Note that the choice of a single-lane tunnel in the present study was largely due to the experimental constraints of the present TRAIN rig. From the viewpoint of applied aerodynamics application, the lateral dynamics induced by a platoon running through the tunnel are of more interest, especially when the platoon enters/leaves the tunnel and passes other vehicles. However, such kind of experiments requires to conduct in a multi-lane tunnel, which is technically inaccessible at this stage. Some two-lane test will be conducted in future after improving the present TRAIN rig facility.

Figure 1: Photographs of the platform and the lorry platoon on the train rig.

The vehicle model was a 1/20th scale commercial box-type lorry (see Figure 2), with the length(L), width(W) and height(H) being 0.395 m, 0.125 m and 0.175 m, respectively. This lorry model was simplified from a typical commercial vehicle Leyland DAF 45-130, which has been extensively investigated either as a single–vehicle (Cheli et al., 2011; Patel et al., 2019; Quinn et al., 2007) or in a platoon formation (He et al., 2019; Robertson et al., 2019). Therefore, there are abundant

results to offer useful references and necessary validations of the present experiments and numerical simulations. Furthermore, by using the same vehicle shape as in previous studies by the same research group (He et al., 2019; Robertson et al., 2019), we can make direct comparisons of the results obtained in the tunnel and in the open air, which is the focus of the present study. Note that some detailed features of the original lorry, such as side mirrors and windshield overhangs, were removed or simplified in the present lorry model. This simplification is related to the simulation efforts, as including these features has a negligible effect on the aerodynamic performance, but it would require intensive meshing design and result in an exponential growth in the number of mesh cells.

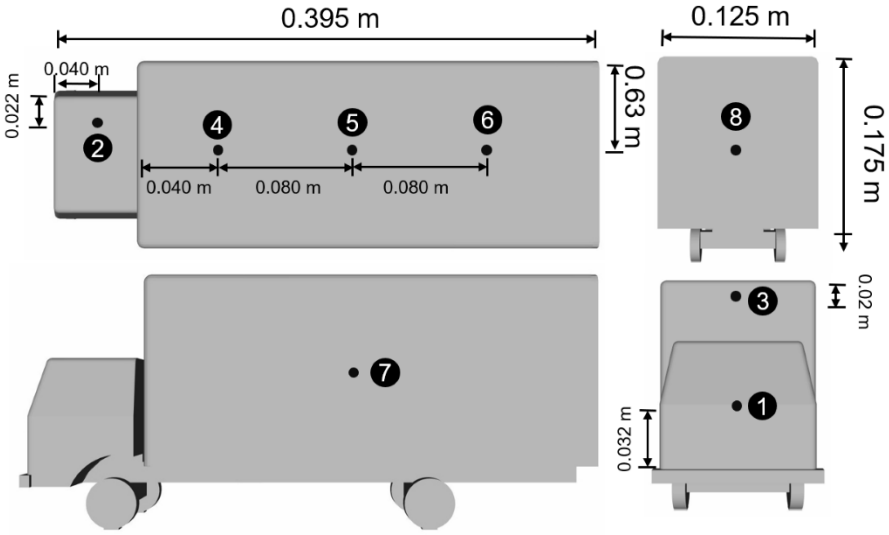

Figure 2: The shape and dimensions of the reduced-scale lorry model. The positions of the pressure taps for surface pressure measurements are indicated by the numbers on the lorry.

The chosen number of eight lorries in the platoon was based on the requirement for a fully developed boundary layer (Robertson et al., 2019; Soper et al., 2014). In the present study, the inter-lorry distance was fixed at $1.5L$ for all the experiments. Note that this separation distance can reflect typical road conditions more appropriately. It is not uncommon for lorries to travel at a separation comparable to this distance, while smaller separations could only be achieved through autonomous vehicle technology. It is also worth mentioning that the aerodynamics of platoons in the open air were qualitatively similar for different separation distances from $0.5L$ to $1.5L$ (Robertson et al., 2019). Therefore, the selection of the separation distance ~~has~~was not ~~been~~ a major concern~~ed factor~~ in the present study. The focus of this study is to compare different behaviours of lorry platoons in the tunnel and in the open air. The lorry platoon was propelled at a speed of $V_{plat} = 25 \pm 1$ m/s, corresponding to a Reynolds number of 2.96×10^5 based on the lorry's height H. The actual speed was monitored with an accuracy of ± 0.10 m/s by a series of position finders and reflectors mounted on the suspended ground plane. Because of the aerodynamic drag on the lorry models and the friction between the vehicle

206 mounting point and the rig, there is a slight decrease in the speed (1.17 m/s) of the
207 lorry platoon when it left the tunnel.

208

Probe number	Height from the ground level (y/H)	Distance from the lorry body side (z/H)
A	0.86	0.14
B	0.45	0.14
C	0.11	0.14
D	0.86	0.28

209 Table 1: The positions of the multi-hole probes for measuring the slipstream properties. Here, H is
210 the height of the lorry model.

211 A coordinate system was defined such that the x-axis was aligned in the direction
212 of platoon motion; the y-axis was in the vertical direction measured from the ground
213 plane; the z-axis was on the horizontal plane and perpendicular to the direction of
214 platoon motion. The slipstream velocities and pressures were measured by multi-
215 hole probes (Turbulent Flow Instrumentation Series 100 Cobra probes). This kind of
216 probe can measure three velocity components of the airflow and also the static
217 pressure, with the accuracies being 0.3 m/s and $\pm$5 Pa for velocity and pressure
218 measurements, respectively. All data were recorded at a sampling frequency of
219 5kHz and filtered using a 650 Hz low-pass filter to reflect the maximum frequency
220 response of the probe. The multi-hole probe has a $\pm$45 degree cone of acceptance,
221 which is sufficient to capture the majority flow around the lorries (Robertson et al.,
222 2019). The slipstream data were measured at a series of positions as shown in Table
223 1. The surface pressure on each lorry was measured by an on-board pressure
224 monitoring system as described by (Robertson et al., 2019). Metal tubing adaptors,
225 acting as pressure taps, were glued into the lorry walls and connected to the pressure
226 transducer (manufactured by FirstSensor) via silicon tubes. The data was sampled
227 by a stand-alone data logger as a series of voltages and then converted to pressure
228 with an accuracy of $\pm$15 Pa with careful calibration. The surface pressure
229 measurements were made at eight different locations as indicated in Figure 2. Note
230 that both the platoon configuration and the data acquisition details in the present
231 work were in line with previous studies of a lorry platoon in the open air (He et al.,
232 2019; Robertson et al., 2019), so that a direct comparison between the behaviours in
233 the tunnel and in the open air can be made.

234

235

2.2. Data analysis methodology

Due to the highly temporal variations in velocity and pressure obtained from individual measurement, multiple runs (of the order of 10~20) are required to ~~conduct such~~ ensure that the standard deviation of the ensemble average is comparable to the turbulence level (Baker et al., 2001). Therefore, 20 runs of the experiment were conducted in the present study to ensure statistically converged ensemble averages (Robertson et al., 2019; Sterling et al., 2008). In addition, as the sampling rate was constant but the platoon speed varied between runs, the positions of the lorries where the measurements were taken were unique for each run. To eliminate this problem, all the data ~~was~~ were re-sampled to a nominal speed of 25 m/s. The raw data ~~was~~ were re-aligned with the sample points when the first lorry entered the tunnel. The slipstream velocity and pressure are presented in dimensionless form.

$$U(\tau) = \frac{u(\tau)}{V_{plat}} \tag{1}$$

$$V(\tau) = \frac{v(\tau)}{V_{plat}} \tag{2}$$

$$W(\tau) = \frac{w(\tau)}{V_{plat}} \tag{3}$$

$$U_{res}(\tau) = \sqrt{(\frac{u(\tau)}{V_{plat}})^2 + (\frac{v(\tau)}{V_{plat}})^2} \tag{4}$$

$$C_p(\tau) = \frac{p(\tau) - p_0}{1/2\rho V_{plat}^2} \tag{5}$$

Here, $\tau = V_{plat}t/L$ is the normalised time in terms of the nominal platoon speed V_{plat} and the lorry model's length L. Note that τ is taken as zero when the first lorry enters the tunnel for presenting the slipstream properties of the platoon, or when each lorry enters the tunnel for presenting their surface pressures and drag properties. U, V and W represent the normalised velocity for the longitudinal, lateral and vertical components, respectively. U_{res} is the overall normalised horizontal velocity. The pressure coefficient C_p is calculated with respect to an ambient reference pressure p_0 and the air density ρ. The atmospheric pressure was measured by a GBP3300 Digital Barometer with an accuracy of $\pm$200 Pa. The temperature and humidity were measured by an Oregon Scientific BAR208HGA weather station. The surface pressure of each lorry is presented in term of pressure coefficient as well. The uncertainty in C_p for surface pressure measurements (see, for example, the error bars in Figure 18), is calculated as the sum of the bias limit (which accounts

for the performance limits of the equipment) and random uncertainty (which accounts for run-to-run variability due to the unsteadiness in the airflow).

3. Numerical set-up

3.1. Simulation methodology and numerical schemes

The simulation approach adopted in the present study was IDDES, Improved Delayed Detached Eddy Simulation. This approach was originated from the Detached Eddy Simulation (DES) proposed by (Spalart et al., 1997). DES can reduce the high computational cost for high Reynolds number flows, but it has disadvantages in certain aspects such as modelling stress depletion and grid-induced separation. IDDES solves these problems nicely, thus it is particularly suitable for studying mixed flows with both attached and separated regions.

The simulations were performed by commercial CFD software ANSYS 18.2 using a pressure-based solver with the finite volume method. The SIMPLE (Semi-Implicit Method for Pressure-Linked Equations) algorithm was used to handle the pressure and velocity coupling equations. The IDDES approach, based on the model by (Gritskevich et al., 2012)), was adopted and the bounded central differencing was applied to the momentum equations. An implicit scheme with second-order accuracy was applied to the time term. The time step was set to 1×10^{-4}s (Hemida and Krajnović, 2009; Niu et al., 2017) and there were 50 iterations in each time step.

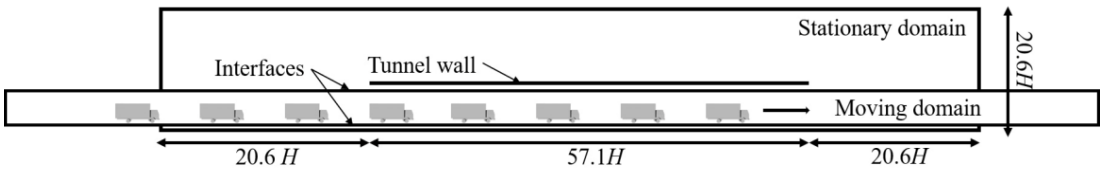

Figure 3: Computational domain for lorries in platoon travelling through a tunnel.

3.2. Computational domain and boundary condition

The computational domain consists of both stationary and moving sub-domains with the width being 41.14H. For the other dimensions of the domain, please refers to Figure 3. In order to accurately simulate the relative motion between the vehicles and the tunnel, the sliding mesh technique was adopted. This technique is promising in solving the problems similar to the present study (Chen et al., 2017; Chu et al., 2014; Liu et al., 2014; Niu et al., 2017). To be specific, during the simulation, the moving sub-domain slides relative to stationary sub-domain along the interfaces without mesh generation at every time step, and thus the nodes do not need to be re-aligned at the interfaces. In each time step, the fluxes across each grid point inside the non-conformal interface zones were computed.

The initial conditions were set to zero gauge pressure and zero velocity in both moving and stationary sub-domains. The top and side faces of the stationary sub-domain were set to zero static pressure. A non-slip boundary condition was applied to the lorry surface, tunnel walls and the ground of the stationary sub-domain. In order to ensure that the flow field is fully developed and to avoid the impact of the boundary conditions, the simulation started when the first lorry was outside the tunnel at a distance of $20.6H$ away from the entrance and stopped when the last lorry was outside the tunnel at a distance of $20.6H$ away from the exit.

3.3. Mesh generation scheme

Figure 4 shows the computational meshes used in this study. The structured meshing method was employed for the entire computational domain by the commercial software Ansys ICEM-CFD. The total number of mesh cells used in this study was 34.9 million. Another two meshes with different numbers of cells (17.4 million and 24.2 million) were used to test the mesh sensitivity (see Table 2). The Courant-Friedrichs-Lewy number (CFL$= U_\infty \Delta t/\Delta x$, where Δx is the length of cells and Δt is the time step) remained below 1 with a small number of localised exceptions. (Xia et al., 2017)) and (Wang et al., 2017)) have shown that this minor infringement on the CFL requirement is unlikely to affect the simulation results.

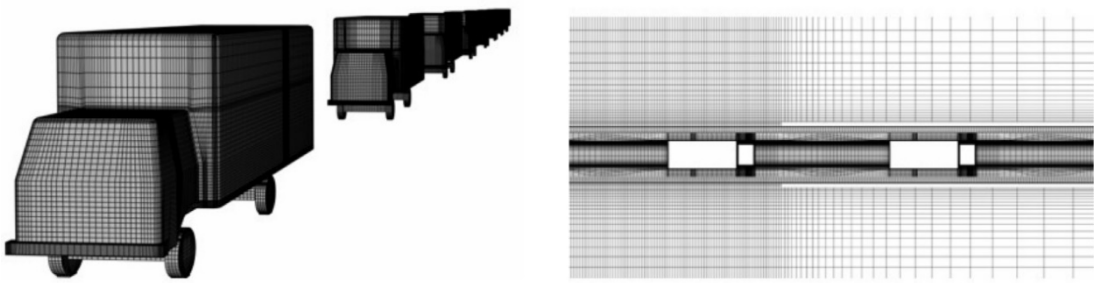

Figure 4: Computational meshes used in this study: (a) lorry surface; (b) horizontal cross-section of the whole domain at $y/H = 0.57$.

	Coarse	Medium	Fine
Averaged y+	49	45	33
Number of mesh cells used in the moving domain (million)	12.2	14.7	20.3
Number of mesh cells used in the stationary domain (million)	5.2	9.5	14.6
Total number of mesh cells (million)	17.4	24.2	34.9

Table 2: The parameters for the grid sensitivity testing in the simulations.

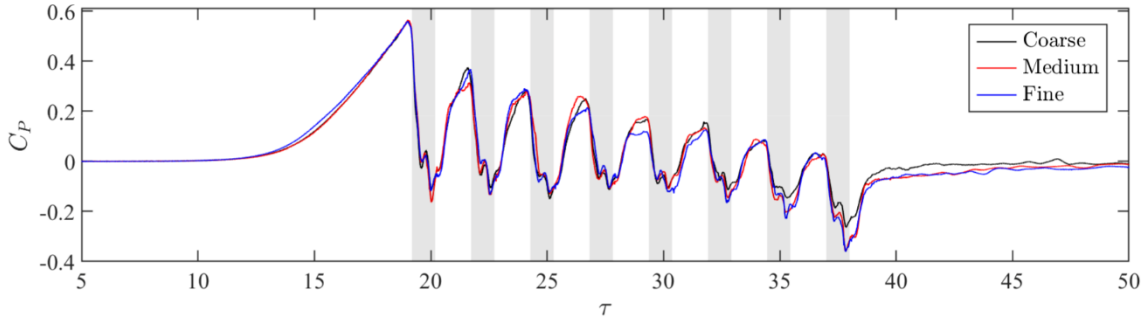

Figure 5: Pressure coefficients for different mesh densities. The shaded rectangles indicate the time duration for each lorry to pass the probes.

The pressure coefficients C_p of the IDDES simulations based on three different numbers of cells are shown in Figure 5. The testing point is located at a position of $0.45H$ above the ground and $0.14H$ away from the lorry body. The differences in the positive pressure peaks between the fine and middle meshes are relatively small. However, the results using coarse mesh have relatively large deviations, especially at $37 < \tau < 38$. Therefore, the fine mesh was used in this study.

3.4. Validation of simulation results

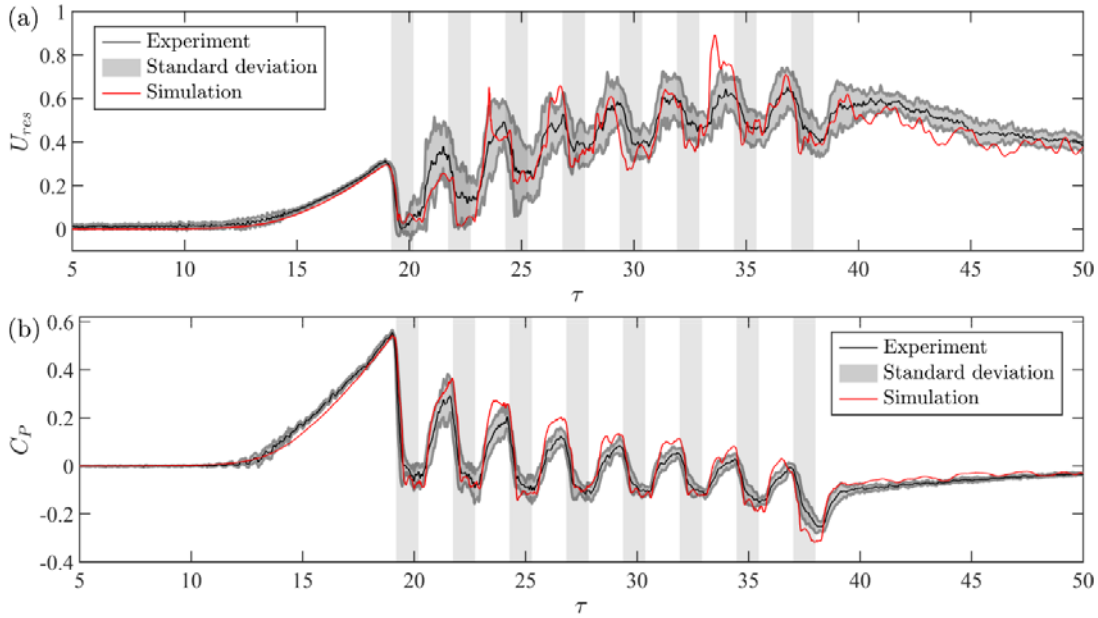

Figure 6: Comparison between the experiments and numerical simulations measured at the position of the multi-hole probe B (see Table 1): (a) normalised horizontal velocity; (b) pressure coefficient. The shaded rectangles indicate the time duration for each lorry to pass the probes.

To validate the CFD results, we show in Figure 6 the simulated normalised velocities and pressure coefficients at the position of multi-hole probe B (see Table 1) together with the experimental data. The trends of the pressure data obtained from the numerical simulations are consistent with the experimental results. Whilst the velocity data deviate a lot in detail, the numerical data mostly fall within one standard deviation of the experimental values. To understand the discrepancy in

velocity data, we note that although the gap in the ground plane has been modelled in the simulations, the exact boundary conditions for this region are difficult to define. In addition, the tunnel is assumed to be fully sealed in the simulations, which is impossible in the experiments. Another possible reason could come from the multi-hole probe. The velocity component in the direction of platoon motion is sensitive to the alignment of the probe. The ± 45 degree cone of acceptance of the probe might also restrict the detection of air flows (Soper, 2016; Soper et al., 2017).

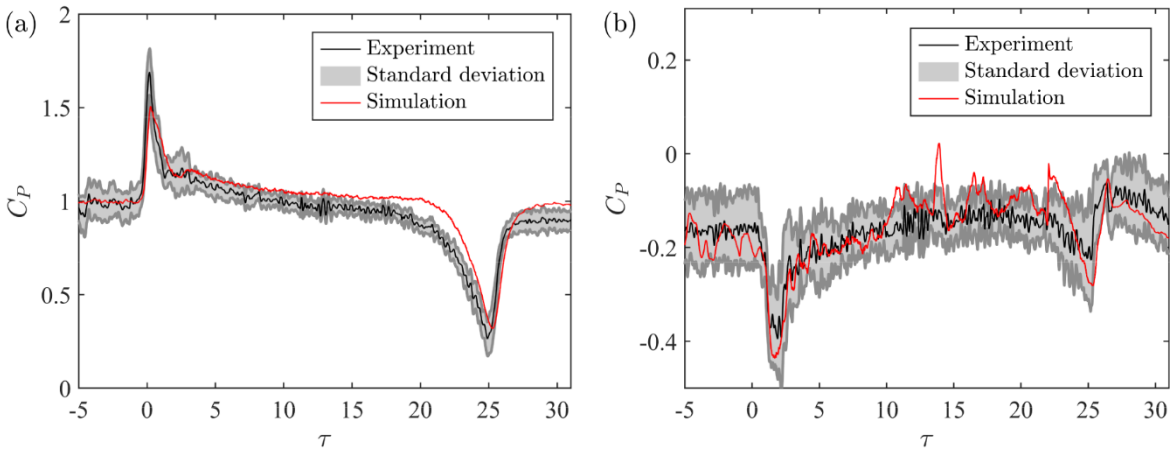

Figure 7: The surface pressure coefficients from the experiments and simulations. The monitoring positions are at (a) point No.1 and (b) point No.8 as indicated in Figure 2.

Figure 7 compares the surface pressure coefficients between the simulations and the experiments. Figure 7(a) and (b) represent the data at the cab front and rear points of the leading lorry, respectively. It is seen in Figure 7(a) that the data from the numerical simulations compare well with the experimental results. When the lorry is running inside the tunnel, the simulated frontal surface pressure decreases slower than the experimental cases. This can be ascribed to a gradual decrease in the speed of the platoon in the experiments (as a result of the rig friction and the aerodynamic drag aforementioned), in contrast to the constant speed used in the simulations. The experimentally measured C_p drops from around 1 prior to the inlet to around 0.9 after leaving the tunnel (beyond $\tau = 27$), suggesting that the platoon speed at the exit is 95% of that at the entry. Indeed, direct measurement with laser sensors shows that the platoon speed reduces by 4.6%, which provides ~~a~~ support for the conclusion that the lower C_p of the experiments is due to the slowing down of the lorry model when running through the tunnel. For the rear region of the lorry where separated flow exists (Figure 7(b)), the simulation data are also in good agreement with the experimental values (typically within one standard deviation).

The last important quantity to be validated is the mean drag coefficient as defined below:

$$C_d = \frac{F}{0.5\rho V_{plat}^2 A_f} \tag{6}$$

Here, F is the effective drag force, and A_f is the reference area derived from the projected area of the lorry. V_{plat} is the nominal platoon speed aforementioned. Note that the calculation of mean drag coefficient requires integrating pressure over a discrete geometry of the lorry surface and thus sufficient data should be acquired to make the integration (Dorigatti et al., 2015). In this work, the pressures along the lorry surface were experimentally measured at eight positions only. This low resolution of pressure data prevents us from obtaining a reliable drag coefficient. Therefore, we validate the numerical model here by comparing the drag coefficient simulated in the open air with the experimental results obtained by (Robertson et al., 2019)). The error bars in Figure 8 indicate the root-mean-square (rms)~~rms~~ magnitudes for the simulations, while for the experiments they are uncertainties calculated by applying the uncertainty transfer formula based on the uncertainties of the pressure coefficients at all the locations. It is seen that there is a discrepancy between the experimental and numerical results, which may be due to the relatively low resolution of surface pressure taps in the experiments. As noted by (Robertson et al., 2019)), the experimental data only provides an estimated drag coefficient and the uncertainty may be less than the true error, because the assumption of uniform pressure across the discretised area might be inaccurate. Nevertheless, it will be shown in Section 4.3 that there is a good agreement between the experimental and IDDES values in the surface pressure coefficients for lorries both inside the tunnel and in the open air (see, for example, Figure 18). This gives us confidence in the reliability of the present results.

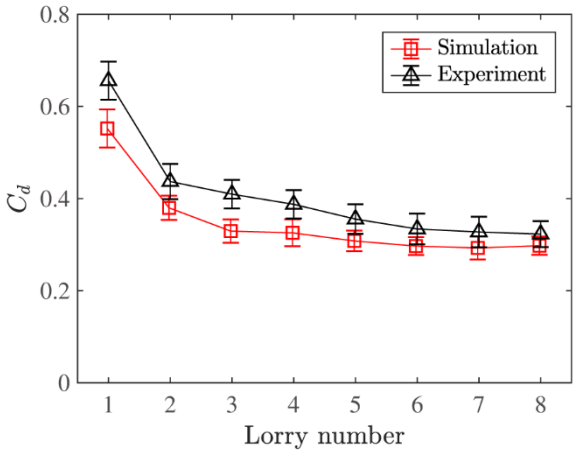

Figure 8: Mean drag coefficient in the open air from the experiments and simulations. The experimental results were obtained by (Robertson et al., 2019).

4. Results and discussion

4.1. Slipstream properties

We first show in Figure 9 the aerodynamic flow around the lorry platoon, in terms of the normalised horizontal velocity in the slipstream. The data measured in

the tunnel and in the open air are plotted together for comparison. In the open air, the flow created by the moving platoon is characterised by a continually growing boundary layer punctuated with pulse peaks near the front of each lorry (Robertson et al., 2019). While in the tunnel, the piston effect induced by the movement of the lorry platoon causes the bulk flow through the tunnel. Therefore, the horizontal velocity starts rising long before the arrival of the first lorry. The bulk flow in the tunnel also leads to a smaller approach flow velocity for the platoon. Fluctuations are recorded due to the complex flow patterns. The peaks associated with the lorries are more obvious in the tunnel than in the open air. It is further seen that the horizontal velocity does not approach the maximum value until the sixth lorry passes, suggesting that at least this number of vehicles are needed to study the aerodynamic phenomena of a long platoon in the tunnel.

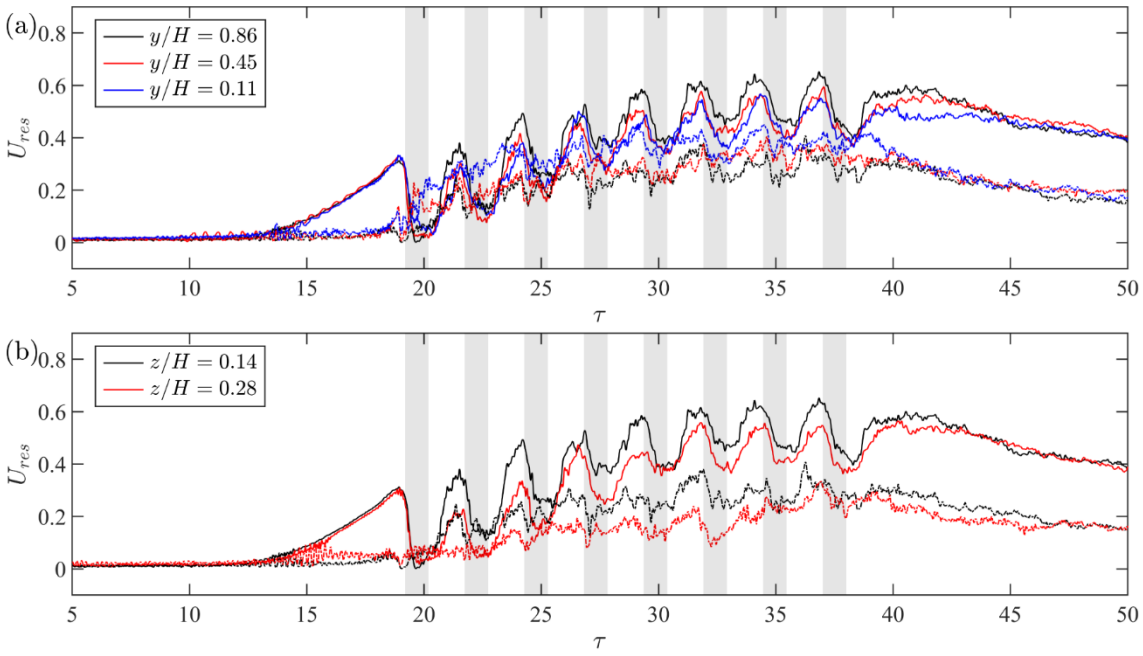

Figure 9: The experimentally measured normalised horizontal velocity as a function of the normalised time: (a) at various heights from the ground level with the same location of $z/H = 0.14$ away from the lorry side; (b) at different locations away from the lorry side with the same height of $y/H = 0.86$ from the ground level. The solid lines denote the results obtained in the tunnel and the dotted lines denote the results obtained in the open air (Robertson et al., 2019). The shaded rectangles indicate the time duration for each lorry to pass the probes.

Figure 10 presents the experimental pressure coefficients at different heights from the ground level and at different distances away from the lorry. Also shown in the figure are the experimental data for the same platoon configuration running in the open air. The pressure coefficients for different positions have a similar trend as time evolves. To be specific, the pressure coefficients rise until the first lorry arrives at the positions where the cobra probes were installed. When the first lorry passes by the cobra probes, the slipstream pressures due to the so-created turbulent flow have lower values than the ambient fluid. The pressure coefficients therefore drop drastically after the first lorry leaves the location of the probes. As the platoon

moves forward, all the lorries induce similar variations in the local pressure. Thus, there are eight peaks as seen in the figure, corresponding to eight lorries in the platoon. These phenomena are the same in both the tunnel and the open air.

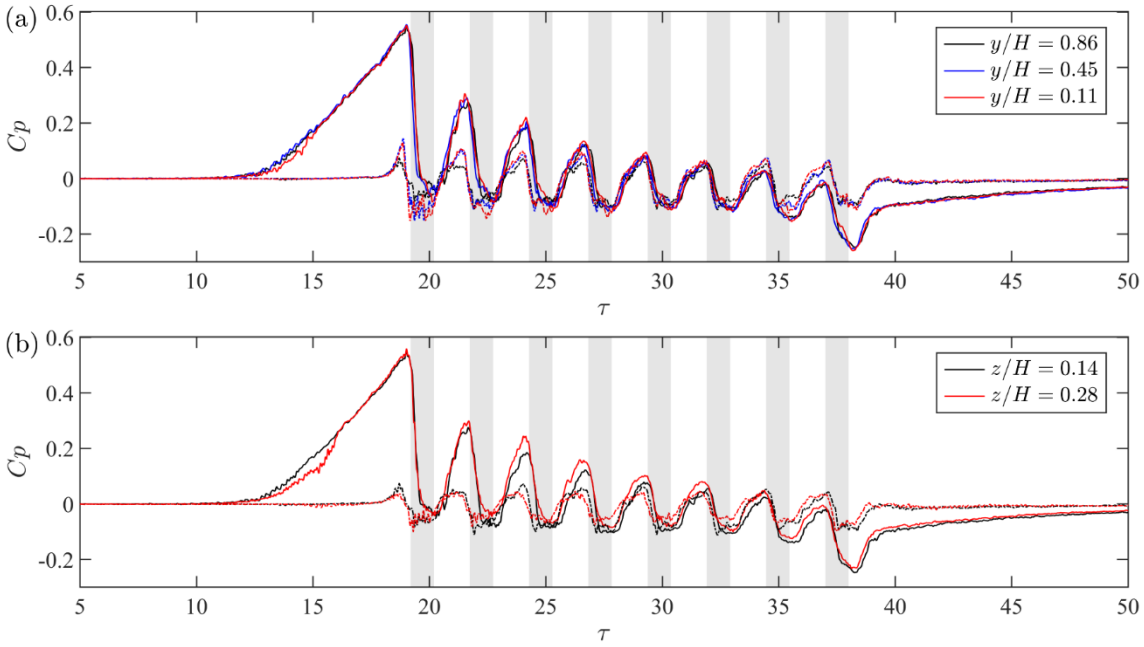

Figure 10: The temporal variations of the experimentally measured pressure coefficients: (a) at different heights from the ground level with the same location of $z/H = 0.14$ away from the lorry side; (b) at different locations away from the lorry side with the same height of $y/H = 0.86$ from the ground level. The solid lines denote the results obtained in the tunnel and the dotted lines denote the results obtained in the open air (Robertson et al., 2019). The shaded rectangles indicate the time duration for each lorry to pass the probes.

However, when considering the magnitude of the pressure coefficient, significant differences are observed between the data in the tunnel and in the open air. When the platoon runs in the tunnel, the air around the lorries is largely forced to flow parallel to the travelling direction of the platoon because of the spatial confinement. This results in a slower dissipation in the frontal pressure. Therefore, the first peak of pressure coefficient reaches a value as large as 0.55 in the tunnel, while the value in the open air is about four times lower. This difference gets progressively smaller for the following lorries and the pressure coefficients for different situations become almost identical for the fifth to seventh lorries in the platoon. On the other hand, as less airflow is able to penetrate into the rear region of the platoon in the tunnel, the low-pressure behind the last lorry is strongly intensified, leading to a great fall in the value of pressure coefficient (as low as -0.25). This is in strong contrast to the almost constant value (around -0.1) of the negative peaks for the platoon in the open air. Note that the above differences in the pressure coefficient are observed for all the positions shown in Figure 10. These much larger pressure variations in the tunnel indicate that additional aerodynamic forces exist when the platoon passes by.

To have a better understanding of the aerodynamic flow created by the lorry platoon in the tunnel, we now turn to the numerical results for detail. Figure 11 presents the top view of the horizontal velocity at the height $y/H = 0.57$ above the ground. The transient velocity fields at three distinct times during the platoon passing through the tunnel are shown, together with the stationary results in the open air. The highest speed appears in the rear regions of all the lorries, regardless of in the tunnel or in the open air. However, when the platoon is running inside the tunnel, stronger flows are induced in the frontal and rear regions of the platoon. The velocity in the regions between each lorry is also larger than that in the open air. For the lateral sides of the platoon, the influenced regions expand gradually as the platoon moves forward. While the sides of the first two lorries have a relatively weak airflow, the horizontal velocity around the last four lorries increases to a constant value of 0.6 inside the tunnel. These findings are in good agreement with the experimental results as shown in Figure 9.

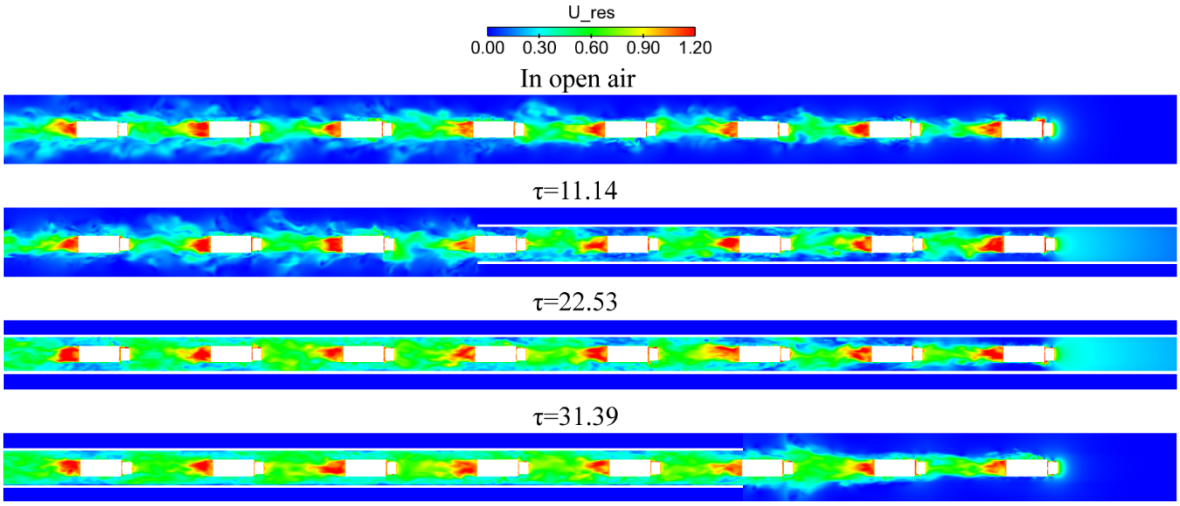

Figure 11: The simulated velocity fields during the lorry platoon passing through the tunnel at three distinct times on the horizontal plane of $y/H = 0.57$. The top panel shows the data in the open air for comparison.

Figure 12 shows the corresponding turbulent kinetic energy (TKE) of the velocity fields in Figure 11. It is seen that intense turbulent kinetic energy is concentrated in the rear regions of all the lorries. This is originated from small-scale turbulent structures due to the large-scale flow separations in these regions. Interestingly, the TKE seems to be weaker for some intermediate lorries in the tunnel than in the open air, suggesting that the transient flow created by these lorries is less fluctuating.

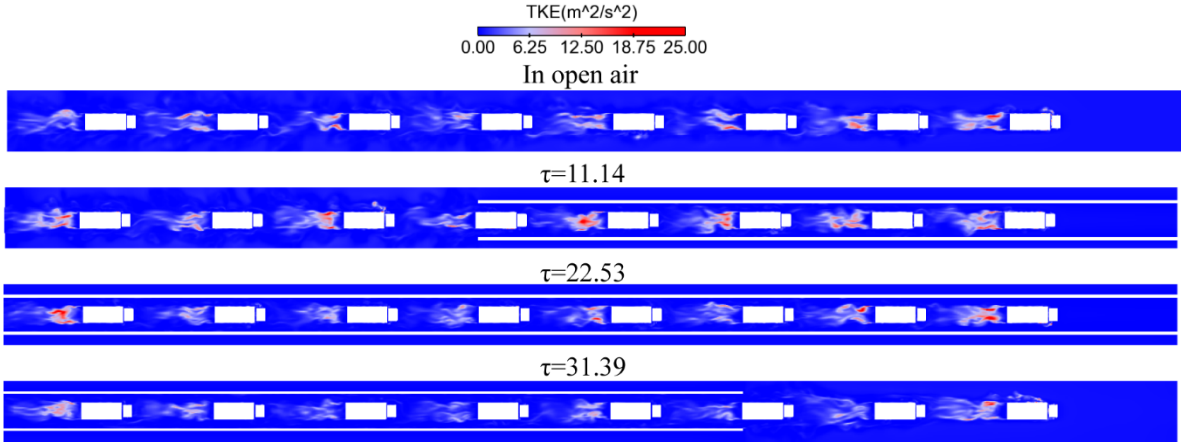

Figure 12: The instantaneous turbulent kinetic energy during the lorry platoon passing through the tunnel at three distinct times on the horizontal plane of $y/H = 0.57$. The top panel shows the data in the open air for comparison.

Figure 13 shows the side view of the pressure distribution at $z/H = 0.076$ during the platoon running through the tunnel and in the open air. The results reveal a significant piston effect induced by the movements of the lorry platoon inside the tunnel. As the platoon enters the tunnel, the pressures at the cab front of the leading lorries increase greatly, especially for the first one. When the whole lorry platoon is inside the tunnel, the frontal positive pressure continuously decreases from the leading lorry to the last one, which is consistent with the experimental results shown in Figure 10. Moreover, the experimentally-observed smaller positive pressure at the front region and larger negative pressure at the rear region of the last lorry are more clear here. As the platoon begins to leave the tunnel, the pressures around the lorries reduce again quickly, with the frontal positive pressures of some lorries (e.g., the second and the third ones) even smaller than those in the open air.

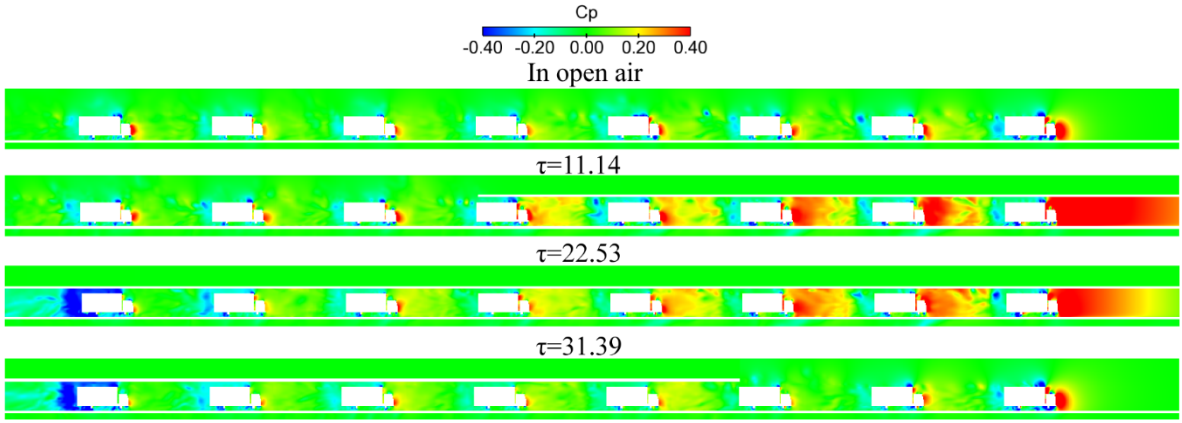

Figure 13: The pressure distribution during the lorry platoon passing through the tunnel at three distinct times on the vertical plane of $z/H = 0.076$. The top panel shows the data in the open air for comparison.

4.2. *Flow structures*

To have a closer look at the aerodynamic flow created by the platoon, we use the iso-surfaces of the second invariant Q to extract the flow structures around the lorries. The second invariant Q is defined as below,

$$Q = -\frac{1}{2}(\bar{S}_{ij}\bar{S}_{ij} - \bar{\Omega}_{ij}\bar{\Omega}_{ij}) \tag{7}$$

where $\bar{S}_{ij}$ and $\bar{\Omega}_{ij}$ are the symmetric and anti-symmetric parts of the velocity gradient tensor. Iso-surfaces with positive Q represent locations where the strength of the rotation overcomes the strain, thus indicating vortical structures (Jeong and Hussain, 1995).

Figure 14 compares the instantaneous flow structures around the first, the fifth and the last lorries running in the middle of the tunnel and in the open air. The distributions of the vortices around the leading lorries are similar in these two cases. As shown in Figure 14 (a) and (b), a large number of vortices are generated around the cab, box side and rear regions, due to the bluff nature of the box lorries. However, some differences in the vortical structures can be found for the platoon in the tunnel: fewer vortices are appearing at the lorry sides. This difference is also observed but less obvious for the fifth and the last lorries as shown in Figure 14 (c) to (f). As mentioned in Section 4.1, the piston effect induced by the movement of the platoon leads to a lower approach velocity, which results in weaker flow separations. Thanks to the shielding effect, there are fewer vortices around the fifth and the last lorries compared to those around the leading lorries in both the tunnel and the open air.

Figure 15 compares the streamlines at the centreline plane in the frontal region of three representative lorries in the platoon. Note that each lorry is in the middle of the tunnel and travelling at the corresponding time in the open air. As clearly indicated in Figure 15 (a) and (d), the recirculation region close to the frontal edge of the lorry box is obviously larger in the open air than in the tunnel. This phenomenon is also identified ~~on~~ in the same region of the fifth lorry (see Figure 15 (b) and (e)). When it comes to the last lorry, the separation almost disappears compared to the leading lorries due to the shielding effect in both the tunnel and the open air. Figure 16 compares the corresponding streamlines in the rear region. The figure shows two counter-rotating recirculation vortices in the near-wake region. The most noticeable difference in the flow structures between the lorries travelling in the tunnel and in the open air is the size of the bottom vortex and the upper vortex. It is clear that the presence of the tunnel enlarges the upper vortices for all the lorries in the tunnel. As will be shown in next section, these differences in flow structures provide direct support for interpreting the surface pressure results.

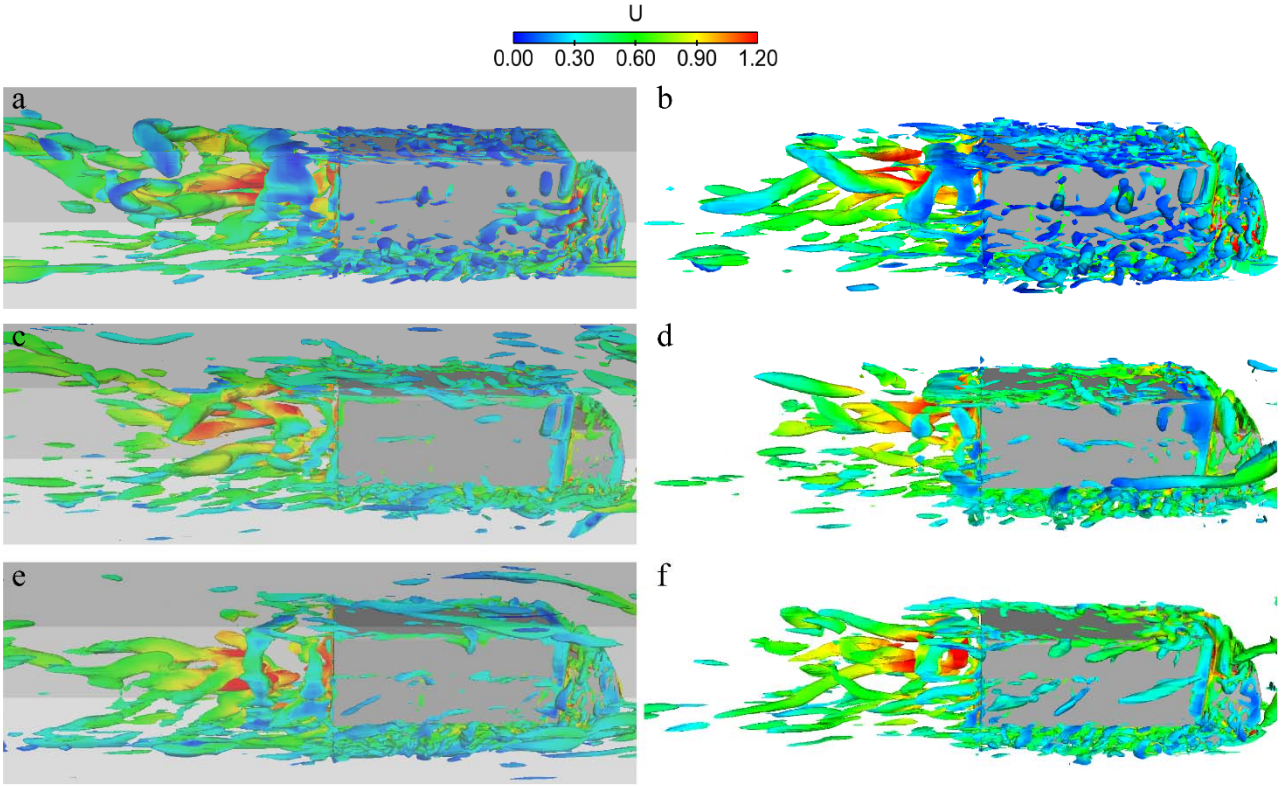

Figure 14: The instantaneous iso-surfaces of the second invariant Q. Left panel: (a), (c) and (e) are the lorries 1, 5 and 8 in the tunnel. Right panel: (b), (d) and (f) are the lorries 1, 5 and 8 in the open air. Here, Q is set to be 50000 s^{-2} and ~~collared~~coloured by the normalised velocity.

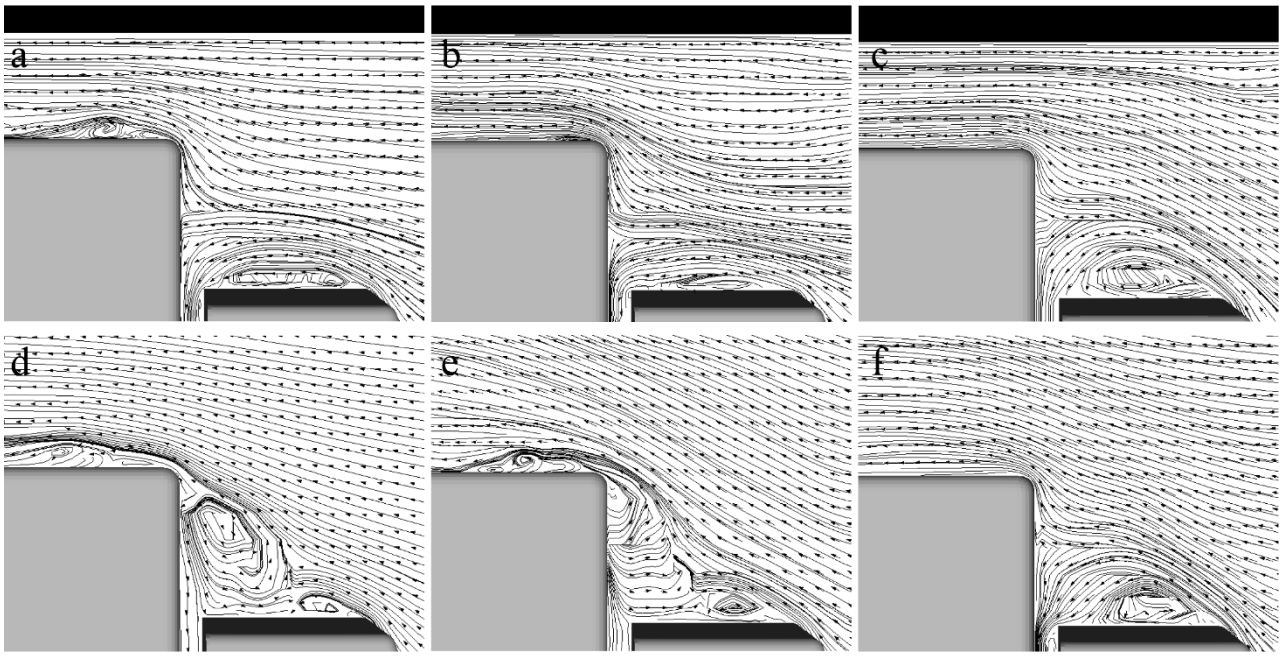

Figure 15: Illustrations of the frontal flow structures of three representative lorries in the platoon at *z/H*=0. Top panel: (a), (b) and (c) are the lorries 1, 5 and 8 in the tunnel. Bottom panel: (d), (e) and (f) are the lorries 1, 5 and 8 in the open air.

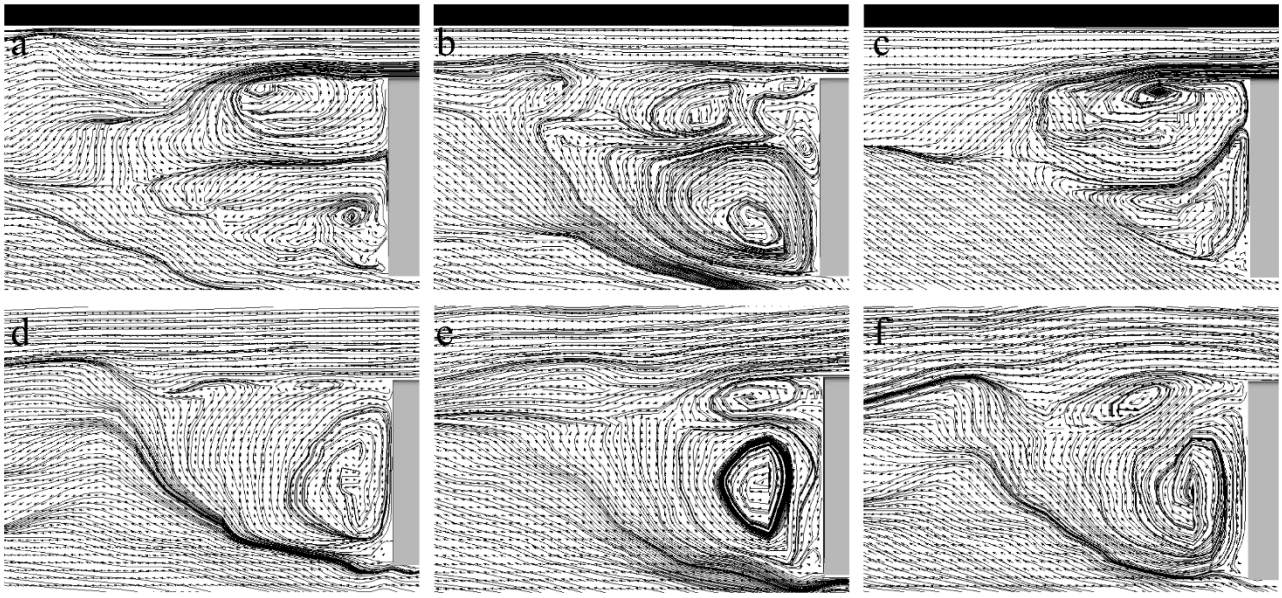

Figure 16: Illustrations of the wake flow structures of three representative lorries in the platoon at z/H=0. Top panel: (a), (b) and (c) are lorries 1, 5 and 8 in the tunnel. Bottom panel: (d), (e) and (f) are lorries 1, 5 and 8 in the open air.

4.3. *Surface pressure analysis*

As the aerodynamic flow created by the platoon running in the tunnel is pronouncedly different from that in the open air, it is natural to expect that the pressure distributions on the lorries' surfaces are also different. However, in contrast to the case in the open air, the flow field around the platoon is strongly unsteady, and the positions of the lorries relative to the tunnel change with time. In order to study the surface pressure variation, a user-defined function was added to the CFD code to simulate the surface pressures on the moving lorries.

Figure 17 presents the time series of the simulated surface pressure coefficient C_p at two typical surface positions of each lorry in the tunnel and in the open air. Note that the data is aligned with respect to the time when each lorry arrives at the entrance of the tunnel. The shielding effect is obvious for the results shown in Figure 17(a) and (b). In the tunnel, the surface pressure on the cab front decreases for the first four lorries, with the largest drop occurring at the second one, and then keeps relatively constant for the last four lorries. Also thanks to the shielding effect, the pressure variations for the trailing lorries in the tunnel are not as drastic as thoseat for the leading lorries during entering and leaving the tunnel. However, frequent and small fluctuations are observed for the trailing lorries in both the tunnel and the open air, which are induced by the separated flow structures from the upwind stream as shown in Figure 14. When it comes to the box rear regions of the lorries in the tunnel (see Figure 17(c)), almost all the lorries experience larger surface pressure fluctuations when entering the tunnel, but only the first and the last lorries have obvious changes in the surface pressure when leaving the tunnel. The last lorry has the lowest rear pressure coefficient in the tunnel, which is consistent

with pressure distribution as shown in Figure 13. In addition, except for the last lorry, ~~which has the lowest pressure coefficient in the tunnel,~~ the pressures on the box rear fluctuate at similar levels for the other lorries.

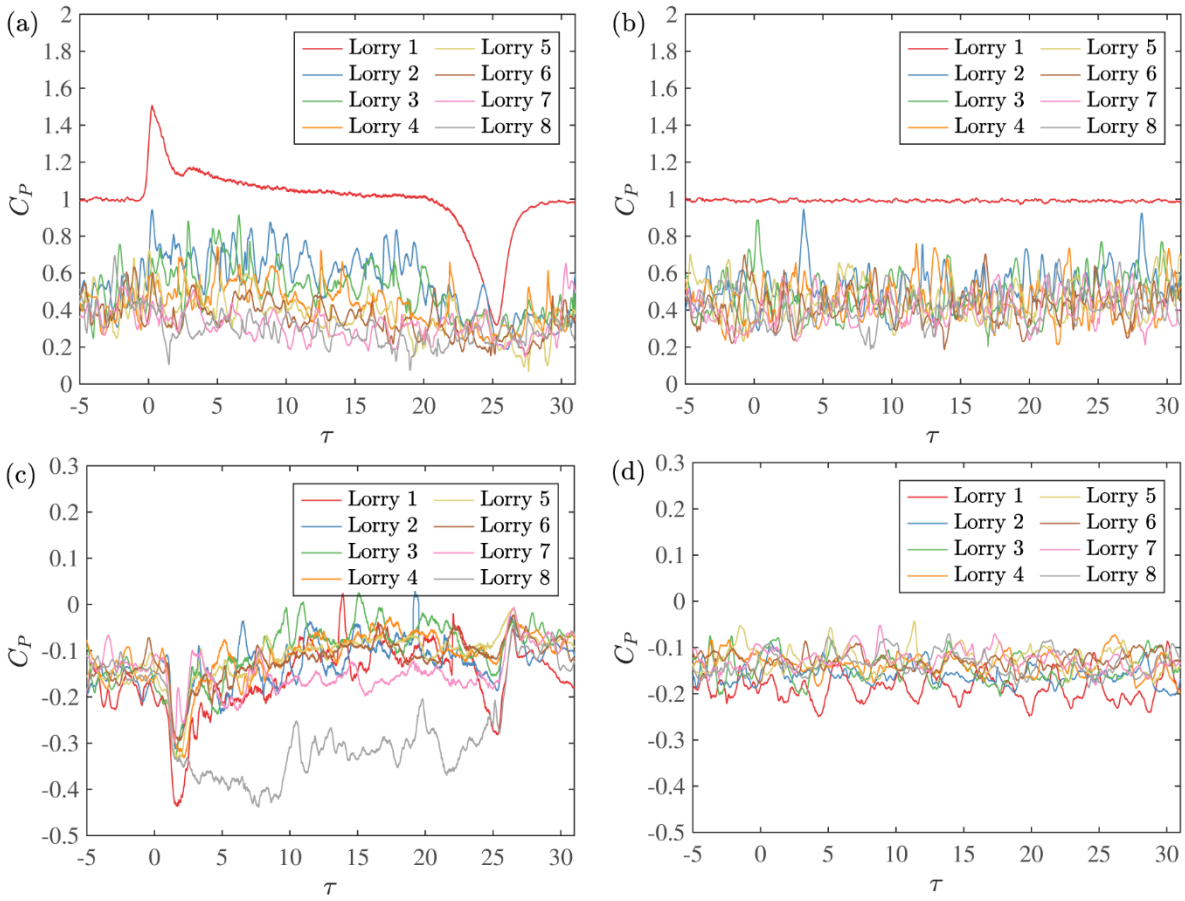

Figure 17: The simulated surface pressure coefficients of all the lorries as a function of the normalised time: (a) cab front in the tunnel; (b) cab front in the open air: (c) box rear in the tunnel; (d) box rear in the open air.

Figure 18 shows the time-averaged surface pressure coefficients of four representative lorries along the central line in the platoon. Both experimental and numerical results are plotted together, and a comparison is made between the data in the tunnel and in the open air (Robertson et al., 2019). Note that the surface pressure coefficient in the tunnel is averaged over the intermediate 4-meters when each lorry is travelling inside the tunnel. The shaded areas are employed to distinguish different regions along the lorry's surface. It is seen that the data predicted by the simulations are generally in good agreement with the experimental data. The mean surface pressure coefficients have a similar trend for different lorries both inside and outside the tunnel. To be specific, the surface pressure along the central line of each lorry drops significantly in the regions where the strongest flow separations occur (see Figures 14-16), ~~as indicated by the negative peaks,~~ and then becomes almost unchanged for the box top and rear regions. Moreover, for both data in the tunnel and in the open air, the trailing lorries have much smaller frontal pressures than the

leading one, and their rear pressures are almost the same. As indicated in section 4.2, the piston effect in the tunnel leads to a lower approach velocity and a weaker flow separation near the box front edge, as compared to the case in the open air. This is evident by the pressure values of the negative peaks: the lowest C_p at the box front edge of Lorry 1 is -2.14 in the tunnel, compared to the value of -3.0 in the open air. C_p at the cab front edge of Lorry 1 is also lower in the open air than that in the tunnel. This difference in the negative pressure peak becomes smaller for the trailing lorries, as a result of shielding. Another appreciative difference that can be found is the surface pressure coefficients of Lorry 8. Their values are systematically lower in the tunnel than in the open air, supported by both the experiments and simulations. However, the difference between the two cases is generally more pronounced at the rear region of the lorry than it is at the front. This suggests that the mean drag coefficient for Lorry 8 will be significantly higher inside the tunnel, as we will show in next section.

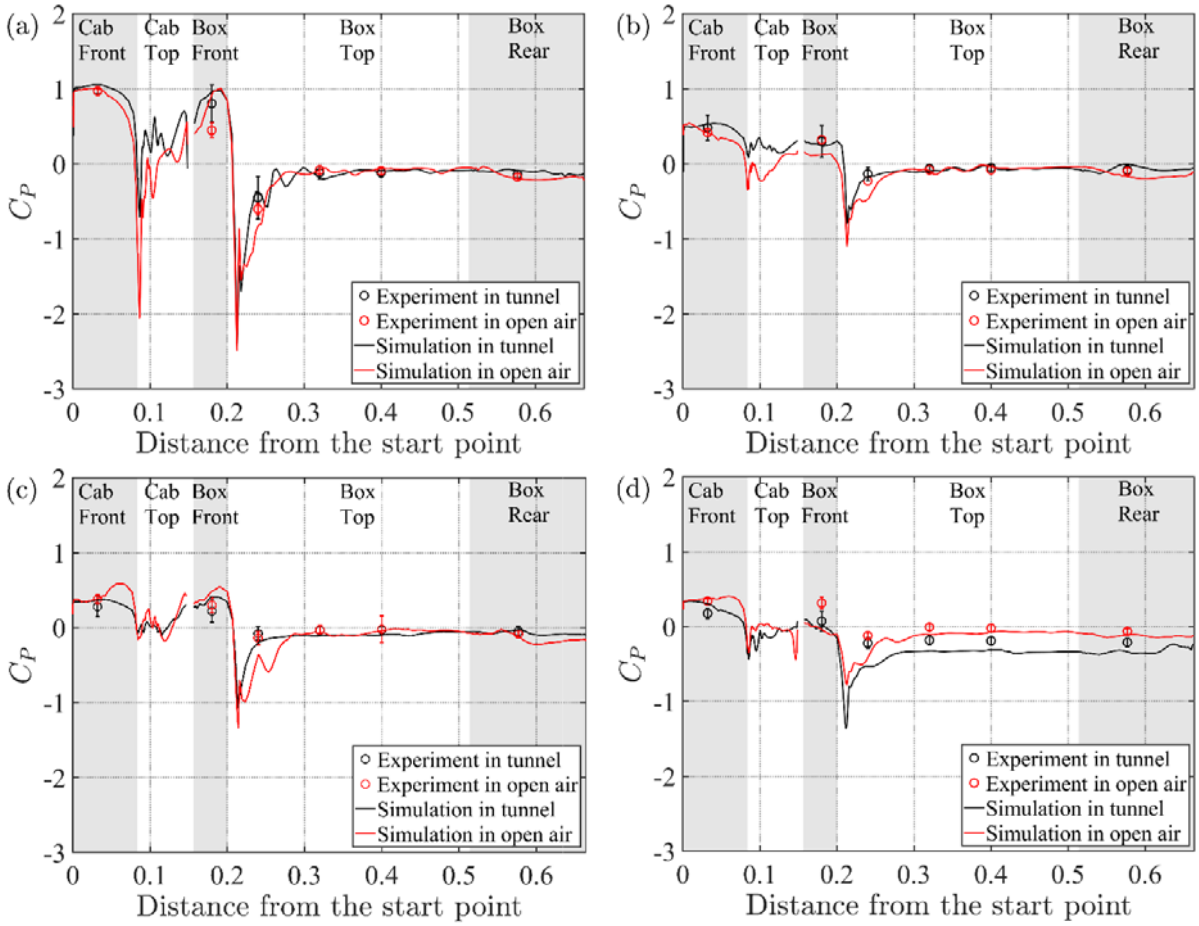

Figure 18: The mean surface pressure coefficients of different lorries along the central line of the platoon: (a) Lorry 1; (b) Lorry 3; (c) Lorry 5; (d) Lorry 8. Both experimental and numerical results are shown for the cases in the tunnel and in the open air. The shaded area is used to help to distinguish different regions along the lorry's surface.

4.4. *Drag analysis*

Now we consider the aerodynamic drag coefficient. Figure 19 illustrates the time series of drag coefficients of each lorry running through the tunnel and in the open air. It is clearly seen in Figure 19(a) that the drag coefficients of all the lorries first rise sharply when entering the tunnel, and then decrease slowly inside the tunnel before a sudden drop at the exit. The variation in the drag coefficients can be up to 70% for the leading lorry in the tunnel, which is absent for the case in the open air (Figure 19(b)). As a benefit from the shielding effect, the trailing lorries in the tunnel experience ~~less~~ smaller ~~drag~~ variation in the drag coefficients, but they still experience larger fluctuations than those in the open air. A similar result was obtained previously by (Li et al., 2010), who simulated a two-vehicle platoon running into a tunnel. Their work showed that the drag coefficient of the trailing vehicle did not change significantly while the drag coefficient of the leading vehicle increased during the process of entering the tunnel. ~~In addition,~~ It is further seen in Figure 19(a) that the drag coefficient continuously decreases from Lorry 1 to Lorry 5, with the largest drop occurring at the second lorry. Note that the drag coefficient of Lorry 8 in the tunnel is much higher than the other lorries, in contrast to the case in the open air. This is largely due to the strongly negative rear pressure when the lorry travels through the tunnel, as shown in Figures 17(c) and 18(d).

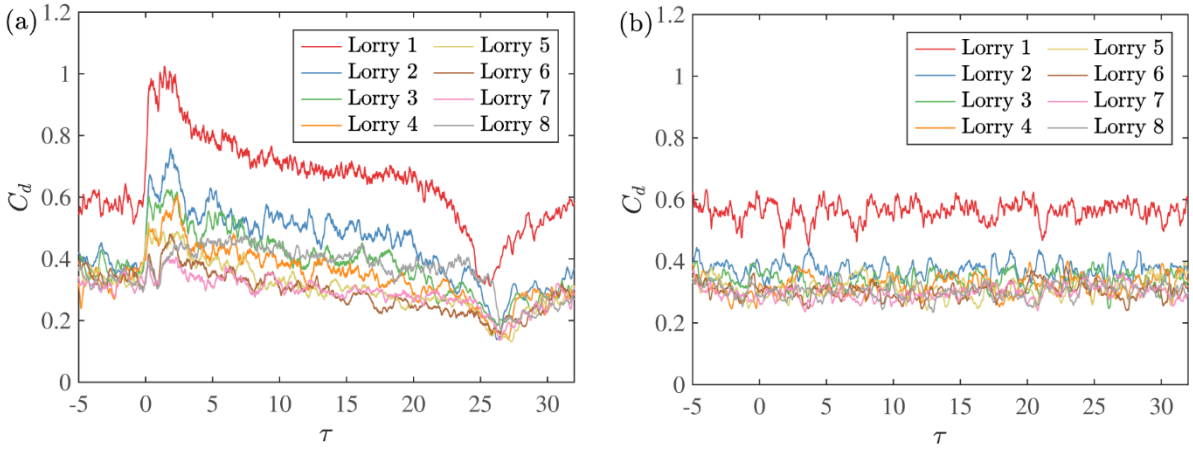

Figure 19: The time series of drag coefficients of different lorries in the platoon: (a) in the tunnel and (b) in the open air.

In order to compare the drag coefficients in the tunnel and in the open air directly, we show in Figure 20(a) the corresponding mean values. Note that the drag coefficients in the tunnel are averaged for the intermediate duration when the whole platoon is travelling inside the tunnel. It is seen that while the mean drag coefficient in the open air only changes significantly for the first three lorries and approaches a plateau after that, C_d in the tunnel continues to decrease appreciably until the fifth lorry. For the first four lorries, the presence of the tunnel tends to increase the drag coefficient due to the much higher frontal pressure, thus the C_d values in the tunnel are larger than those in the open air. The drag coefficients from the fifth to the

seventh lorries are almost identical for different situations. However, for the last lorry in the tunnel, there is a large increase in the drag coefficient due to the strongly negative rear pressures. It is worth noting that whilst the drag coefficient is typically higher for a platoon travelling inside a tunnel than it is in the open air, the same is also true for vehicles travelling in isolation. The drag coefficient of an isolated lorry $C_{d-single}$ is 0.98 inside the tunnel and 0.64 in the open air. Therefore, to compare the benefits of platooning inside the tunnel and in the open air, it is instructive to normalise the drag coefficient by that of an isolated vehicle in their respective cases, as shown in Figure 20(b). It is seen that platooning provides a drag-reduction benefit for all the lorries in both the tunnel and the open air. Interestingly, there is a much larger drag reduction due to platooning for the lorries inside the tunnel than those in the open air. This difference is as large as 20% for the lorries towards the middle of the platoon. Furthermore, the absolute difference between drag coefficients for a lorry in the platoon and in isolation is always higher in the tunnel than it is in the open air.~~in the tunnel and in the open air is higher for a single vehicle than it is for all the vehicles in the platoon,~~ This suggest~~sing~~ that platooning has a greater potential for reducing fuel consumption in the tunnel than in the open air.

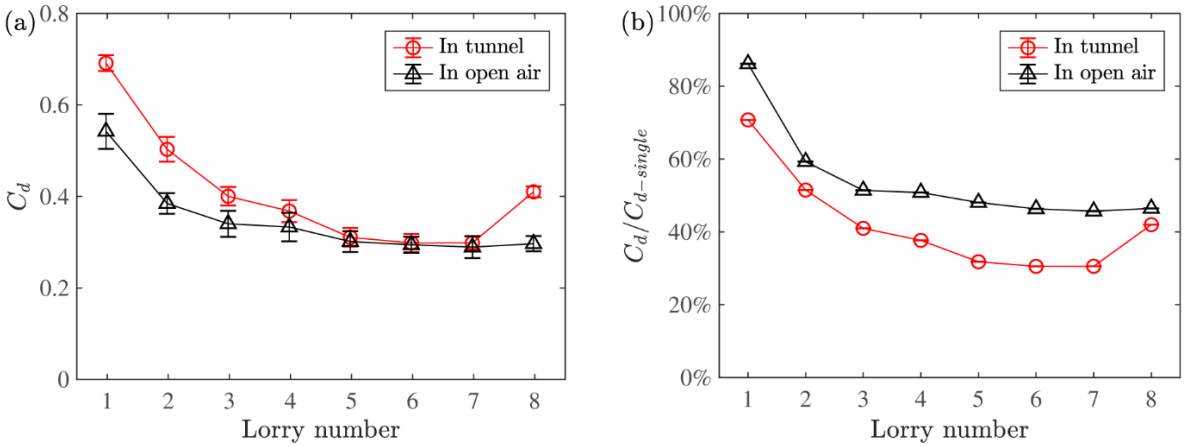

Figure 20: A comparison of (a) the mean drag coefficients and (b) the drag reduction ratio $C_d/C_{d-single}$ between the lorries in platoon in the tunnel and in the open air.

5. Conclusion

This paper presents a detailed experimental and numerical study of the aerodynamic phenomena of a long lorry platoon running through a tunnel. The slipstream properties, surface pressure and drag force are discussed and compared to the data obtained in the open air. The main findings of this study are as follow.

- Due to the piston effect, stronger flows are induced in the frontal and rear regions of the platoon in the tunnel than in the open air. The influenced regions expand faster when the platoon is travelling inside the tunnel.

Both experimental and numerical results reveal greater static pressure variations near the frontal regions of the leading lorries and the rear region of the last lorry in the tunnel.

- The flow structures around the lorry platoon are altered due to the tunnel walls: Fewer vortices are generated from the front edge of the lorry, and larger upper vortices are observed in the rear region. A weaker flow separation leads to a smaller drop in the surface pressure near the box front edge, as compared to the case in the open air.

- The variations of the drag coefficients show similar behaviours with the surface pressure, exhibiting great variations while entering and leaving the tunnel. In contrast to the case in the open air, the mean drag coefficient in the tunnel is no longer monotonically decreasing from the first to the last lorry in the platoon. Rather, it significantly decreases to a plateau at the fifth lorry and then increases again greatly at the last lorry due to strongly negative rear pressures.

- All vehicles, in both the tunnel and the open air, experience a reduction in drag due to platooning. The drag is consistently higher in the tunnel than in the open air for both isolated vehicles and platoons. However, the drag reduction due to platooning is consistently greater in the tunnel than ~~it is~~ in the open air. This implies a greater potential to reduce fuel consumption in the tunnel than in the open air.

Finally, we would like to highlight three issues for future study of vehicle platoons in a tunnel. The first one is the inter-vehicle separation distance, which was fixed at 1.5 vehicle-length in the present study. However, autonomous vehicle technologies allow smaller separation distances. Therefore, examining platoons with different separation distances is definitely an important issue to explore. The second one is the vehicle shape. The vehicle model used in the present study is a representative of regional delivery trucks. For long-haul transportation trucks, they are often longer with taller cabs and can be expected to behave differently in a tunnel. So studying the tunnel effects on platoons with different vehicle shapes is also desirable. The third one is the tunnel geometry. Due to experimental constraints, the present study was conducted in a single-lane tunnel. However, tunnels with multiple lanes are of more interest for aerodynamics applications. Platoons travelling through such tunnels would produce different flow fields from the one encountered here. Therefore, studying platoons travelling through a multi-lane tunnel is also an important issue and should be conducted in future.

6. Acknowledgements

We are grateful to the anonymous referees, whose comments led to significant improvements of our paper. And we thank Mingzhe He for his help in the experiments. This work was supported by an EPSRC funded project entitled `The aerodynamics of close running ground vehicles - EP/N004213/' and the Department of Science and Technology of Guangdong Province (Grant No. 2019B21203001). The authors also would like to thank the computational support from BlueBEAR at the University of Birmingham and the Center for Computational Science and Engineering at Southern University of Science and Technology.

7. References

Alam, A. Al, Gattami, A., Johansson, K.H., 2010. An experimental study on the fuel reduction potential of heavy duty vehicle platooning, in: 13th International IEEE Conference on Intelligent Transportation Systems. IEEE, pp. 306–311. https://doi.org/10.1109/ITSC.2010.5625054

Armagan, A., Onur, Y., Habib, U., Altinisik, A., Yemenici, O., Umur, H., 2015. Aerodynamic Analysis of a Passenger Car at Yaw Angle and Two-Vehicle Platoon. J. Fluids Eng. 137, 121107. https://doi.org/10.1115/1.4030869

Baker, C.J., Dalley, S.J., Johnson, T., Quinn, A., Wright, N.G., 2001. The slipstream and wake of a high-speed train. Proc. Inst. Mech. Eng. Part F J. Rail Rapid Transit 215, 83–99. https://doi.org/10.1243/0954409011531422

Bonnet, C., Fritz, H., 2000. Fuel Consumption Reduction in a Platoon: Experimental Results with two Electronically Coupled Trucks at Close Spacing, in: SAE Technical Papers. https://doi.org/10.4271/2000-01-3056

Browand, F., Mcarthur, J., Radovich, C., 2004. Fuel Saving Achieved in the Field Test of Two Tandem Trucks, UC Berkeley: California Partners for Advanced Transportation Technology.

Cheli, F., Corradi, R., Sabbioni, E., Tomasini, G., 2011. Wind tunnel tests on heavy road vehicles: Cross wind induced loads—Part 1. J. Wind Eng. Ind. Aerodyn. 99, 1000–1010. https://doi.org/10.1016/j.jweia.2011.07.009

Chen, T.Y., Lee, Y.T., Hsu, C.C., 1998. Investigations of piston-effect and jet fan-effect in model vehicle tunnels. J. Wind Eng. Ind. Aerodyn. 73, 99–110. https://doi.org/10.1016/S0167-6105(97)00281-X

Chen, Z., Liu, T., Zhou, X., Niu, J., 2017. Impact of ambient wind on aerodynamic performance when two trains intersect inside a tunnel. J. Wind Eng. Ind.

744 Aerodyn. 169, 139–155. https://doi.org/10.1016/j.jweia.2017.07.018

745 Chu, C.-R., Chien, S.-Y., Wang, C.-Y., Wu, T.-R., 2014. Numerical simulation of
746 two trains intersecting in a tunnel. Tunn. Undergr. Sp. Technol. 42, 161–174.
747 https://doi.org/10.1016/j.tust.2014.02.013

748 Chung, C.-Y., Chung, P.-L., 2007. A Numerical and Experimental Study of
749 Pollutant Dispersion in a Traffic Tunnel. Environ. Monit. Assess. 130, 289–299.
750 https://doi.org/10.1007/s10661-006-9397-0

751 Davila, A., Aramburu, E., Freixas, A., 2013. Making the Best Out of Aerodynamics:
752 Platoons, in: SAE Technical Papers. https://doi.org/10.4271/2013-01-0767

753 Dorigatti, F., Sterling, M., Baker, C.J., Quinn, A.D., 2015. Crosswind effects on the
754 stability of a model passenger train—A comparison of static and moving
755 experiments. J. Wind Eng. Ind. Aerodyn. 138, 36–51.
756 https://doi.org/10.1016/j.jweia.2014.11.009

757 Eftekharian, E., Abouali, O., Ahmadi, G., 2015. An improved correlation for
758 pressure drop in a tunnel under traffic jam using CFD. J. Wind Eng. Ind.
759 Aerodyn. 143, 34–41. https://doi.org/10.1016/j.jweia.2015.04.013

760 Gritskevich, M.S., Garbaruk, A. V., Schütze, J., Menter, F.R., 2012. Development
761 of DDES and IDDES Formulations for the k-ω Shear Stress Transport Model.
762 Flow, Turbul. Combust. 88, 431–449. https://doi.org/10.1007/s10494-011-
763 9378-4

764 He, M., Huo, S., Hemida, H., Bourriez, F., Robertson, F.H., Soper, D., Sterling, M.,
765 Baker, C., 2019. Detached eddy simulation of a closely running lorry platoon. J.
766 Wind Eng. Ind. Aerodyn. 193, 103956.
767 https://doi.org/10.1016/j.jweia.2019.103956

768 Hemida, H., Krajnović, S., 2009. Transient Simulation of the Aerodynamic
769 Response of a Double-Deck Bus in Gusty Winds. J. Fluids Eng. 131, 0311011–
770 03110110. https://doi.org/10.1115/1.3054288

771 Humphreys, H., Bevly, D., 2016. Computational Fluid Dynamic Analysis of a
772 Generic 2 Truck Platoon, in: SAE Technical Papers.
773 https://doi.org/10.4271/2016-01-8008

774 Jang, H.-M., Chen, F., 2002. On the determination of the aerodynamic coefficients
775 of highway tunnels. J. Wind Eng. Ind. Aerodyn. 90, 869–896.
776 https://doi.org/10.1016/S0167-6105(02)00156-3

777 Jang, H.-M., Chen, F., 2000. A novel approach to the transient ventilation of road
778 tunnels. J. Wind Eng. Ind. Aerodyn. 86, 15–36. https://doi.org/10.1016/S0167-

779 6105(99)00135-X

780 Jeong, J., Hussain, F., 1995. On the identification of a vortex. J. Fluid Mech. 285,
781 69. https://doi.org/10.1017/S0022112095000462

782 Lammert, M.P., Duran, A., Diez, J., Burton, K., Nicholson, A., 2014. Effect of
783 Platooning on Fuel Consumption of Class 8 Vehicles Over a Range of Speeds,
784 Following Distances, and Mass. SAE Int. J. Commer. Veh. 7, 2014-01–2438.
785 https://doi.org/10.4271/2014-01-2438

786 Le Good, G., Resnick, M., Boardman, P., Clough, B., 2018. Effects on the
787 Aerodynamic Characteristics of Vehicles in Longitudinal Proximity Due to
788 Changes in Style, in: SAE Technical Papers. https://doi.org/10.4271/2018-37-
789 0018

790 Li, L., Du, G.-S., Li, Y.-W., Liu, Z.-G., 2009. Numerical Simulation of the
791 Transient Aerodynamic Phenomena Associated with a Van Running Into a
792 Road Tunnel, in: 2009 Asia-Pacific Power and Energy Engineering Conference.
793 IEEE, pp. 1–4. https://doi.org/10.1109/APPEEC.2009.4918542

794 Li, L., Du, G., Liu, Z., Lei, L., 2010. The Transient Aerodynamic Characteristics
795 Around Vans Running Into a Road Tunnel. J. Hydrodyn. 22, 283–288.
796 https://doi.org/10.1016/S1001-6058(09)60056-1

797 Liang, K.Y., Mårtensson, J., Johansson, K.H., 2016. Heavy-Duty Vehicle Platoon
798 Formation for Fuel Efficiency. IEEE Trans. Intell. Transp. Syst. 17, 1051–1061.
799 https://doi.org/10.1109/TITS.2015.2492243

800 Liu, Y., Hemida, H., Liu, Z., 2014. Large eddy simulation of the flow around a train
801 passing a stationary freight wagon. Proc. Inst. Mech. Eng. Part F J. Rail Rapid
802 Transit 228, 535–545. https://doi.org/10.1177/0954409713488096

803 McAuliffe, B.R., Ahmadi-Baloutaki, M., 2018. A Wind-Tunnel Investigation of the
804 Influence of Separation Distance, Lateral Stagger, and Trailer Configuration on
805 the Drag-Reduction Potential of a Two-Truck Platoon. SAE Int. J. Commer.
806 Veh. 11, 125–150. https://doi.org/10.4271/02-11-02-0011

807 Niu, J., Zhou, D., Liu, T., Liang, X., 2017. Numerical simulation of aerodynamic
808 performance of a couple multiple units high-speed train. Veh. Syst. Dyn. 55,
809 681–703. https://doi.org/10.1080/00423114.2016.1277769

810 Pagliarella, R.M., 2009. On the Aerodynamic Performance of Automotive Vehicle
811 Platoons Featuring Pre and Post-Critical Leading Forms. Ph.D. thesis. RMIT
812 University.

813 Patel, N., He, M., Hemida, H., Quinn, A., 2019. Large-Eddy Simulation of the

airflow around a truck. J. Wind Eng. Ind. Aerodyn. 195, 104017. https://doi.org/10.1016/j.jweia.2019.104017

Quinn, A.D., Sterling, M., Robertson, A.P., Baker, C.J., 2007. An investigation of the wind-induced rolling moment on a commercial vehicle in the atmospheric boundary layer. Proc. Inst. Mech. Eng. Part D J. Automob. Eng. 221, 1367–1379. https://doi.org/10.1243/09544070JAUTO537

Robertson, F.H., Bourriez, F., He, M., Soper, D., Baker, C., Hemida, H., Sterling, M., 2019. An experimental investigation of the aerodynamic flows created by lorries travelling in a long platoon. J. Wind Eng. Ind. Aerodyn. 193, 103966. https://doi.org/10.1016/j.jweia.2019.103966

Robertson, F.H., Soper, D., Baker, C., 2021. Unsteady aerodynamic forces on long lorry platoons. J. Wind Eng. Ind. Aerodyn. 209, 104481. https://doi.org/10.1016/j.jweia.2020.104481

Sambolek, M., 2004. Model testing of road tunnel ventilation in normal traffic conditions. Eng. Struct. 26, 1705–1711. https://doi.org/10.1016/j.engstruct.2004.06.001

Schito, P., Braghin, F., 2012. Numerical and Experimental Investigation on Vehicles in Platoon. SAE Int. J. Commer. Veh. 5, 2012-01–0175. https://doi.org/10.4271/2012-01-0175

Shladover, S.E., Desoer, C.A., Hedrick, J.K., Tomizuka, M., Walrand, J., Zhang, W.-B., McMahon, D.H., Peng, H., Sheikholeslam, S., McKeown, N., 1991. Automated vehicle control developments in the PATH program. IEEE Trans. Veh. Technol. 40, 114–130. https://doi.org/10.1109/25.69979

Song, X., Zhao, Y., 2019. Numerical investigation of airflow patterns and pollutant dispersions induced by a fleet of vehicles inside road tunnels using dynamic mesh Part II: Pollutant dispersion and exposure levels. Atmos. Environ. 210, 198–210. https://doi.org/10.1016/j.atmosenv.2019.04.028

Soper, D., 2016. The Aerodynamics of a Container Freight Train, Springer Theses. Springer International Publishing, Cham. https://doi.org/10.1007/978-3-319-33279-6

Soper, D., Baker, C., Sterling, M., 2014. Experimental investigation of the slipstream development around a container freight train using a moving model facility. J. Wind Eng. Ind. Aerodyn. 135, 105–117. https://doi.org/10.1016/j.jweia.2014.10.001

Soper, D., Gallagher, M., Baker, C., Quinn, A., 2017. A model-scale study to assess the influence of ground geometries on aerodynamic flow development around a

train. Proc. Inst. Mech. Eng. Part F J. Rail Rapid Transit 231, 916–933. https://doi.org/10.1177/0954409716648719

Spalart, P.R., Jou, W.H., Strelets, M.K., Allmaras, S.R., 1997. Comments on the feasibility of LES for wings and on a hybrid RANS/LES approach. Adv. DNS/LES 1, 4–8.

Sterling, M., Baker, C.J., Jordan, S.C., Johnson, T., 2008. A study of the slipstreams of high-speed passenger trains and freight trains. Proc. Inst. Mech. Eng. Part F J. Rail Rapid Transit 222, 177–193. https://doi.org/10.1243/09544097JRRT133

Tsuei, L., Savaş, Ö., 2001. Transient aerodynamics of vehicle platoons during in-line oscillations. J. Wind Eng. Ind. Aerodyn. 89, 1085–1111. https://doi.org/10.1016/S0167-6105(01)00073-3

Wang, F., Wang, M., Wang, Q., Zhao, D., 2014. An improved model of traffic force based on CFD in a curved tunnel. Tunn. Undergr. Sp. Technol. 41, 120–126. https://doi.org/10.1016/j.tust.2013.12.006

Wang, S., Bell, J.R., Burton, D., Herbst, A.H., Sheridan, J., Thompson, M.C., 2017. The performance of different turbulence models (URANS, SAS and DES) for predicting high-speed train slipstream. J. Wind Eng. Ind. Aerodyn. 165, 46–57. https://doi.org/10.1016/j.jweia.2017.03.001

Watkins, S., Vino, G., 2008. The effect of vehicle spacing on the aerodynamics of a representative car shape. J. Wind Eng. Ind. Aerodyn. 96, 1232–1239. https://doi.org/10.1016/j.jweia.2007.06.042

Xia, C., Wang, H., Shan, X., Yang, Z., Li, Q., 2017. Effects of ground configurations on the slipstream and near wake of a high-speed train. J. Wind Eng. Ind. Aerodyn. 168, 177–189. https://doi.org/10.1016/j.jweia.2017.06.005

Yakhot, V., Orszag, S.A., 1986. Renormalization-Group Analysis of Turbulence. Phys. Rev. Lett. 57, 1722–1724. https://doi.org/10.1103/PhysRevLett.57.1722

Zabat, M., Stabile, N., Farascaroli, S., Browand, F., 1995. The aerodynamic performance of platoons: A Final Report. California Partners for Advanced Transportation Technology, UC Berkeley.